

Tunable Spin-Orbit Torques in Cu-Ta Binary Alloy Heterostructures

Tian-Yue Chen, Chun-Te Wu, Hung-Wei Yen, and Chi-Feng Pai*

Department of Materials Science and Engineering, National Taiwan University, Taipei 10617, Taiwan

The spin Hall effect (SHE) is found to be strong in heavy transition metals (HM), such as Ta and W, in their amorphous and/or high resistivity form. In this work, we show that by employing a Cu-Ta binary alloy as buffer layer in an amorphous $\text{Cu}_{100-x}\text{Ta}_x$ -based magnetic heterostructure with perpendicular magnetic anisotropy (PMA), the SHE-induced damping-like spin-orbit torque (DL-SOT) efficiency $|\xi_{DL}|$ can be linearly tuned by adjusting the buffer layer resistivity. Current-induced SOT switching can also be achieved in these $\text{Cu}_{100-x}\text{Ta}_x$ -based magnetic heterostructures, and we find the switching behavior better explained by a SOT-assisted domain wall propagation picture. Through systematic studies on $\text{Cu}_{100-x}\text{Ta}_x$ -based samples with various compositions, we determine the lower bound of spin Hall conductivity $|\sigma_{SH}| \approx 2.02 \times 10^4 [\hbar / 2e] \Omega^{-1} \cdot \text{m}^{-1}$ in the Ta-rich regime. Based on the idea of resistivity tuning, we further demonstrate that $|\xi_{DL}|$ can be enhanced from 0.087 for pure Ta to 0.152 by employing a resistive TaN buffer layer.

* Email: cfpai@ntu.edu.tw

The spin Hall effects (SHE) [1-3] in heavy transition metals (HM) are known to be strong enough to generate sizable pure spin currents from charge currents for SHE-induced spin-orbit torque (SOT) switching [4,5], magnetic oscillations [6,7], as well as chiral domain wall motion [8,9] on the adjacent ferromagnetic (FM) layers. The phenomenology of the SHE-generated transverse spin current (density) J_s in a HM/FM heterostructure can be described by $J_s = (\hbar / 2e) T_{\text{int}}^{\text{HM|FM}} \theta_{\text{SH}}^{\text{HM}} J_e^{\text{HM}}$, where $\theta_{\text{SH}}^{\text{HM}}$ and J_e^{HM} represent the spin Hall ratio of HM layer and the longitudinal charge current density therein, respectively. $T_{\text{int}}^{\text{HM|FM}}$ is the spin transparency at the HM|FM interface [10], which takes any possible spin backflow [11] and/or spin memory loss [12] at the interface into account ($T_{\text{int}}^{\text{HM|FM}} = 1$ for the 100% spin transmission case). The resulting damping-like (DL) SOT efficiency acting upon the FM layer therefore can be expressed as $\xi_{\text{DL}} \equiv (2e / \hbar) J_s / J_e^{\text{HM}} = T_{\text{int}}^{\text{HM|FM}} \theta_{\text{SH}}^{\text{HM}}$ [13]. Among all HMs, 5d transition metals such as Pt [14], β -Ta [5], and β -W [15] related magnetic heterostructures are found to have giant DL torque efficiencies ($|\xi_{\text{DL}}| \sim 0.10 - 0.30$) due to their strong intrinsic spin-orbit interactions. It has also been shown that 5d HM-related alloys and oxides can generate sizable SHE and even possess greater spin Hall ratios than pure HMs. For instance, Hf(Al)-doped Pt [16], Au-doped Pt [17], PtMn [18], W-doped Au [19], and WO_x [20] all show larger spin Hall ratios or $|\xi_{\text{DL}}|$ while compare to their pure HM counterparts. Even by oxidizing or doping dopants into light transition metals such as Cu, the spin Hall ratio can be significantly enhanced [21,22]. Apparently, engineering spin-Hall

source materials by alloying or oxidation can possibly give rise to a more efficient SOT control over the adjacent FM layers.

In this work, we show that it is possible to linearly tune the DL-SOT efficiency of a magnetic heterostructure by controlling the buffer layer (spin Hall material layer) resistivity. The spin Hall material that we employ is a Cu-Ta binary alloy system, in which the spin Hall ratio can be adjusted by changing the relative $\text{Cu}_{100-x}\text{Ta}_x$ compositions. In Ta-rich regime ($x \geq 84$), the alloy becomes amorphous and serves as a suitable HM buffer layer for generating perpendicular magnetic anisotropy (PMA) for the subsequently deposited FM layer. We first demonstrate current-induced SOT switching in these perpendicularly-magnetized $\text{Cu}_{100-x}\text{Ta}_x/\text{FM}$ heterostructures to verify the existence of giant SHE. Next, we systematically characterize the DL-SOT efficiency $|\xi_{\text{DL}}|$ of these $\text{Cu}_{100-x}\text{Ta}_x/\text{FM}$ heterostructures using the hysteresis loop shift measurements [23]. $|\xi_{\text{DL}}|$ is found to be linearly proportional to the $\text{Cu}_{100-x}\text{Ta}_x$ alloy resistivity, which indicates an intrinsic mechanism and/or side-jump origin of the SHE, with a nearly constant spin Hall conductivity of $|\sigma_{\text{SH}}| \approx 2.02 \times 10^4 [\hbar / 2e] \Omega^{-1} \cdot \text{m}^{-1}$ (lower bound, assuming $T_{\text{int}}^{\text{HM/FM}} = 1$). The critical SOT switching current density J_c of these $\text{Cu}_{100-x}\text{Ta}_x$ -based magnetic heterostructures can further be estimated from the characterized $|\xi_{\text{DL}}|$ and coercive fields H_c , which confirms the domain nucleation/propagation nature of SOT switching in micron-sized PMA devices. Lastly, to demonstrate the benefits of resistivity tuning, we engineer (increase) the resistivity of Ta buffer

layer by nitrogen doping. The maximum DL-SOT efficiency of TaN is found to be $|\xi_{\text{DL}}| = 0.152 \pm 0.006$, while that of Ta control sample is $|\xi_{\text{DL}}| = 0.087 \pm 0.004$.

We prepared our magnetic heterostructures in a high vacuum sputtering chamber with base pressure of 3×10^{-8} Torr. DC and RF magnetron sputtering with 3 mTorr of Ar working pressure were employed for depositions of metallic and oxide (MgO) layers, respectively. The binary alloy buffer layer $\text{Cu}_{100-x}\text{Ta}_x$ was deposited by confocal co-sputtering from a pure Cu and a pure Ta target. The relative compositions can be tuned by the relative sputtering powers of two targets. Multilayer stack heterostructures $\text{Cu}_{100-x}\text{Ta}_x(4)/\text{W}(0.5)/\text{Co}_{20}\text{Fe}_{60}\text{B}_{20}(1.4)/\text{Hf}(0.5)/\text{MgO}(2)/\text{Ta}(2)$ (numbers in the parenthesis are in nm) were deposited onto thermally-oxidized silicon substrates, with x ranges from 20 to 90, as shown in Fig. 1(a). We annealed all our samples at 300 °C for one hour in vacuum to induce PMA of the CoFeB layer. The CoFeB(1.4) layer was sandwiched between a W(0.5) and a Hf(0.5) dusting layer since we found this combination beneficial for obtaining stable PMA for most cases, similar to previous reports [24]. The resistivity of the co-sputtered $\text{Cu}_{100-x}\text{Ta}_x(4)$ layer was characterized by four-point measurements on unpatterned films. As shown in Fig. 1(b), the resistivity of $\text{Cu}_{100-x}\text{Ta}_x$ increases monotonically from 40 $\mu\Omega\text{-cm}$ to 240 $\mu\Omega\text{-cm}$ as we increase the Ta component from 10 at% to 90 at%, which is similar to the trend reported in previous studies [25]. There is also a slope change in the resistivity-to-composition plot at $x \simeq 70$, which indicates a possible transition from poly-crystalline phase to amorphous phase while the alloy is

becoming Ta-rich.

The phase transition of $\text{Cu}_{100-x}\text{Ta}_x$ suggested by the resistivity trend was further verified by the cross-sectional images from high-resolution transmission electron microscopy (HR-TEM), as shown in Fig. 2(a) and (b). In the Cu-rich ($\text{Cu}_{70}\text{Ta}_{30}$) buffer layer, lattice fringes were largely observed but some domains are amorphous, as evidenced by the diffractograms in Fig. 2(a). Hence, the Cu-rich ($\text{Cu}_{70}\text{Ta}_{30}$) buffer layer is mainly polycrystalline with partially-mixed amorphous domains. It should be noted that the spacings of lattice fringes all correspond to the plane spacings of Cu. In contrast, the Ta-rich ($\text{Cu}_{10}\text{Ta}_{90}$) buffer layer has only an amorphous phase as shown in Fig. 2(b). The line-scan profiles (not shown) of the heterostructures also indicate that the Hf and W dusting layers are strongly intermixed with the CoFeB layer, therefore we label the W(0.5)/CoFeB(1.4)/Hf(0.5) layer as an effective ferromagnetic layer “FM” in the TEM images. The microstructure of the $\text{Cu}_{100-x}\text{Ta}_x$ buffer layer significantly affects the resulting magnetic anisotropy of the FM layer above. As presented in Fig. 2(c) and (d), the magneto-optical Kerr effect (MOKE) data clearly show that $\text{Cu}_{70}\text{Ta}_{30}/\text{FM}/\text{MgO}$ is in-plane magnetized while $\text{Cu}_{10}\text{Ta}_{90}/\text{FM}/\text{MgO}$ has PMA. The amorphous nature of the Ta-rich buffer layer makes the $\text{Cu}_{10}\text{Ta}_{90}/\text{FM}$ interface smoother than that of the Cu-rich (poly-crystalline) heterostructure, which is beneficial for obtaining PMA. However, note that for both heterostructures shown here, the MgO layer is not crystalline, which suggests that the crystallinity of oxide layer is not a necessary

condition for getting PMA [26].

Since most of the recent SOT switching studies have focused on magnetic heterostructures with PMA [4,5,27], we now turn our focus on $\text{Cu}_{100-x}\text{Ta}_x/\text{FM}/\text{MgO}$ heterostructures in the Ta-rich regime ($84 \leq x \leq 100$). We prepared Hall-bar samples of $\text{Cu}_{100-x}\text{Ta}_x/\text{FM}/\text{MgO}$ with lateral dimensions of $5\mu\text{m} \times 60\mu\text{m}$ by photolithography and lift-off process. To demonstrate current-induced SOT switching in these heterostructures, as shown in Fig. 3(a), we first applied an in-plane field $H_x = 100\text{Oe}$ to either break the inversion symmetry (single domain picture [28]) or re-align the chiral domain wall moment (multi-domain picture [29]) to facilitate magnetic domain expansion. Then a DC charge current I_{DC} was sent into the current channel of the Hall-bar device to generate a spin current from the SHE of $\text{Cu}_{100-x}\text{Ta}_x$ buffer layer. The resulting SHE-induced SOT acting upon the adjacent FM layer will switch the magnetization when I_{DC} reaches a critical value. All samples with PMA ($84 \leq x \leq 100$) can be reversibly switched by sweeping I_{DC} up to $\pm 5\text{mA}$, and we found critical switching current of all samples to be $\sim \pm 2\text{mA}$ ($J_c \sim \pm 0.8 \times 10^{11} \text{A} \cdot \text{m}^{-2}$). This suggests that the SHE from the $\text{Cu}_{100-x}\text{Ta}_x$ buffer layer is comparable to that from other pure HMs such as Pt, Ta, and W. A representative switching curve from a $\text{Cu}_6\text{Ta}_{94}$ device is shown in Fig. 3(b). The steps observed during current-induced switching can be considered as the evidence of domain wall motion, therefore we believe that the DL-SOT switching observed here is governed by domain nucleation and SOT-assisted domain (wall)

expansion (propagation) [8,23,29].

The results of systematic studies on transport and magnetic properties of $\text{Cu}_{100-x}\text{Ta}_x/\text{FM}/\text{MgO}$ heterostructures as functions of Ta content are summarized in Fig. 4. We first measured the resistance of Hall-bar devices to calculate the resistivity of buffer layer in its amorphous phase. The contribution from the effective FM layer has been subtracted. As shown in Fig. 4(a), the $\text{Cu}_{100-x}\text{Ta}_x$ buffer layer resistivity is linearly proportional to the Ta concentration, which is consistent with the unpatterned film result (the amorphous side of Fig. 1(b)). To systematically characterize the DL-SOT efficiency, we performed the hysteresis loop shift measurements [23,30,31] on $\text{Cu}_{100-x}\text{Ta}_x/\text{FM}/\text{MgO}$ Hall-bar devices. In this type of measurement, the DL-SOT efficiency ξ_{DL} can be estimated from the ratio of measured shift of out-of-plane hysteresis loop H_{eff}^z to the applied current density J_e by [23,32]

$$\xi_{DL} = \frac{2e}{\hbar} \mu_0 M_s (t_{\text{FM}} - t_{\text{dead}}) \cdot \left(\frac{2}{\pi}\right) \cdot \left(\frac{H_{\text{eff}}^z}{J_e}\right), \quad (1)$$

where M_s , t_{FM} , and t_{dead} represent saturation magnetization, nominal thickness, and dead layer thickness of the FM layer, respectively. These parameters are characterized by vibrating sample magnetometer (VSM) from unpatterned films to be $M_s \approx 1500 \text{ emu/cm}^3$ ($1.5 \times 10^6 \text{ A/m}$ in SI units)

and $t_{\text{FM}} - t_{\text{dead}} \approx 0.7 \text{ nm}$. The estimated magnitude of DL-SOT efficiency $|\xi_{DL}|$ is found to be linearly proportional to the Ta content, as shown in Fig. 4(b). Note that the sign of ξ_{DL} is actually negative, consistent with the negative spin Hall ratio of Ta [5]. Since both the resistivity ρ_{CuTa} and DL-SOT efficiency $|\xi_{DL}|$ are proportional to the Ta content of buffer layer, it is obvious that $|\xi_{DL}| \propto \rho_{\text{CuTa}}$ in our heterostructures.

According to the theory of SHE, if the phenomenon is driven by intrinsic mechanism (or side-jump scattering) [1,33] then the spin Hall ratio is related to the spin Hall conductivity σ_{SH} and the conductivity σ_{HM} (or its inverse, resistivity ρ_{HM}) of the HM layer by $\theta_{SH}^{\text{HM}} = \sigma_{SH} / \sigma_{\text{HM}} = \sigma_{SH} \cdot \rho_{\text{HM}}$. The resulting DL-SOT efficiency $|\xi_{DL}| = |T_{\text{int}}^{\text{HM|FM}} \theta_{SH}^{\text{HM}}| \propto |\theta_{SH}^{\text{HM}}| \propto \rho_{\text{HM}}$, provided that the spin transparency at the interface being unchanged. Therefore, our discovery of $|\xi_{DL}| \propto \rho_{\text{CuTa}}$ suggests that the dominating mechanism of the SHE in $\text{Cu}_{100-x}\text{Ta}_x$ buffer layer is intrinsic. By assuming a perfect spin transmission at the HM|FM interface, $T_{\text{int}}^{\text{HM|FM}} = 1$, the lower bound of the spin Hall conductivity is estimated to be $|\sigma_{SH}| \approx 2.02 \times 10^4 [\hbar / 2e] \Omega^{-1} \cdot \text{m}^{-1}$ from the ratio between $|\xi_{DL}|$ and ρ_{CuTa} . If we further assume that the contribution to SHE is solely coming from Ta, then this estimated spin Hall conductivity of Ta is fairly close to the prediction from first-principle calculation [34]. It is also interesting to note that our discovery of a linear dependence between spin Hall ratio and buffer layer resistivity ($|\theta_{SH}^{\text{HM}}| \propto \rho_{\text{HM}}$) is different from the quadratic dependence ($|\theta_{SH}^{\text{HM}}| \propto \rho_{\text{HM}}^2$) reported by Hao and Xiao for Ta-based PMA heterostructures [35], in

which the resistivity was tuned by temperature. However, $|\theta_{SH}^{HM}| \propto \rho_{HM}$ is not an uncommon trend for sputtered heavy transition metals in the moderately dirty (resistive) regime, as can be seen from the cases of Pt [13,36].

We summarize the (out-of-plane) coercive field H_c and the (current-induced SOT) critical switching current density J_c of all $\text{Cu}_{100-x}\text{Ta}_x/\text{FM}/\text{MgO}$ samples with PMA in Fig. 4(c) and (d), respectively. Conventionally, J_c of the current-induced SOT switching in a PMA heterostructure is considered to be related to the DL-SOT efficiency $|\xi_{DL}|$, the effective anisotropy field H_k , and the externally applied in-plane field H_x through [37]

$$J_c = \frac{2e}{\hbar} \mu_0 M_s (t_{\text{FM}} - t_{\text{dead}}) \cdot \left(\frac{H_k}{2} - \frac{H_x}{\sqrt{2}} \right) / |\xi_{DL}|. \quad (2)$$

However, this expression is only suitable for FM layer being single domain such that the switching behavior can be described by a macro-spin model. In most experimental cases, the samples prepared are micron-sized and the magnetization switching process is dominated by domain nucleation and domain wall propagation [23,29,38]. Therefore, in our case, the critical switching current density should be expressed as

$$J_c = \frac{2e}{\hbar} \mu_0 M_s (t_{\text{FM}} - t_{\text{dead}}) \cdot \left(\frac{2}{\pi}\right) \cdot \left(\frac{H_c}{|\xi_{DL}|}\right), \quad (3)$$

in which the coercive field (or the depinning field) H_c and the DL-SOT efficiency $|\xi_{DL}|$ are the two major factors in determining J_c . Using Eqn. (3), we estimated J_c with the data in Fig. 4(b) and (c) and plot the results alongside with the experimentally determined J_c in Fig. 4(d). Though $|\xi_{DL}|$ increases while the buffer layer becomes more Ta-rich, H_c also has a similar growing trend. Therefore, the resulting J_c is almost constant ($\sim 0.8 \times 10^{11} \text{ A} \cdot \text{m}^{-2}$) with respect to the Ta content change. However, our estimation of J_c based on Eqn. (3) clearly reflects the small variations of measured values among different samples, indicating that the SOT switching observed here is indeed better explained by a domain nucleation / domain wall propagation scenario.

In contrast to the Cu-Ta alloy case, in which the buffer layer resistivity is lower than that of pure Ta, we further engineered the buffer layer by nitrogen-doping to see the effects on resistivity enhancement. TaN buffer layer was prepared by reactive sputtering, i.e., flowing both Ar and N₂ gas into the sputter chamber during Ta deposition [39,40]. By adjusting the N₂ flow rate from 0 to 3 sccm (low doping regime) with the Ar flow rate fixed at 30 sccm, we observed a clear quasi-linear resistivity enhancement of the deposited buffer layer, as shown in Fig. 5(a). Note that beyond N₂ flow rate of 3 sccm (high doping regime), the resistivity of TaN has become $\geq 3000 \mu\Omega\text{-cm}$,

much greater than the resistivity of effective FM layer such that most of the applied charge current will be flowing in the FM layer instead of the spin-Hall buffer layer. The same characterization process was performed on TaN/FM/MgO Hall-bar devices and the DL-SOT efficiency $|\xi_{DL}|$ as a function of buffer layer resistivity are summarized in Fig. 5(b), together with the Cu-Ta alloy results. The quasi-linear trends in both $\rho_{CuTa} < \rho_{Ta}$ and $\rho_{TaN} > \rho_{Ta}$ regimes suggest that: (1) The DL-SOT in these heterostructures predominantly originates from the intrinsic SHE of the buffer layers; (2) The DL-SOT efficiency of a Ta-related heterostructure can be engineered by buffer layer resistivity tuning. The maximum DL-SOT efficiency found in TaN-based samples is $|\xi_{DL}| = 0.152 \pm 0.006$, almost two times the pure Ta case ($|\xi_{DL}| = 0.087 \pm 0.004$). Also note that the spin Hall conductivity in the TaN regime (slope of the DL-SOT efficiency to resistivity plot, $|\sigma_{SH}| \approx 1.84 \times 10^3 [\hbar / 2e] \Omega^{-1} \cdot m^{-1}$) is much smaller than that in the Cu-Ta regime. This suggests that although doping can enhance $|\xi_{DL}|$, it could also change the intrinsic property of buffer layer and results in a lower $|\sigma_{SH}|$.

In summary, we report a systematic study on the correlation between DL-SOT efficiency and the buffer layer resistivity through hysteresis loop shift measurements. By varying the resistivity of $Cu_{100-x}Ta_x$ buffer layer, the DL-SOT efficiency in the Ta-rich regime is found to be linearly tunable from $|\xi_{DL}| = 0.039 \pm 0.004$ ($Cu_{84}Ta_{16}$) to $|\xi_{DL}| = 0.087 \pm 0.004$ (pure Ta). The result also suggests an intrinsic SHE mechanism in the Ta-rich buffer layer with a spin Hall conductivity

$|\sigma_{SH}| \approx 2.02 \times 10^4 [\hbar / 2e] \Omega^{-1} \cdot \text{m}^{-1}$ (lower bound). With further systematic studies on TaN buffer layer samples, we demonstrate that the DL-SOT efficiency can also be linearly tuned up to $|\xi_{DL}| = 0.152 \pm 0.006$ by introducing N₂ into Ta in the low doping regime. Our work therefore provides valuable information on the engineering of magnetic heterostructure, especially the spin-Hall buffer layer, to achieve more efficient current-induced SOT switching.

Acknowledgements

This work was supported by the Ministry of Science and Technology of Taiwan under Grant No. MOST 105-2112-M-002-007-MY3. C. F. Pai thank Dr. Kohei Ueda for fruitful discussions.

References

- [1] M. I. Dyakonov and V. I. Perel, *Physics Letters A* **35**, 459 (1971).
- [2] J. E. Hirsch, *Phys Rev Lett* **83**, 1834 (1999).
- [3] S. F. Zhang, *Phys Rev Lett* **85**, 393 (2000).
- [4] I. M. Miron *et al.*, *Nature* **476**, 189 (2011).
- [5] L. Q. Liu, C.-F. Pai, Y. Li, H. W. Tseng, D. C. Ralph, and R. A. Buhrman, *Science* **336**, 555 (2012).
- [6] V. E. Demidov, S. Urazhdin, H. Ulrichs, V. Tiberkevich, A. Slavin, D. Baither, G. Schmitz, and S. O. Demokritov, *Nature Materials* **11**, 1028 (2012).
- [7] L. Q. Liu, C.-F. Pai, D. C. Ralph, and R. A. Buhrman, *Phys Rev Lett* **109**, 186602 (2012).
- [8] S. Emori, U. Bauer, S. M. Ahn, E. Martinez, and G. S. D. Beach, *Nature Materials* **12**, 611 (2013).
- [9] K. S. Ryu, L. Thomas, S. H. Yang, and S. Parkin, *Nature Nanotechnology* **8**, 527 (2013).
- [10] C. F. Pai, Y. X. Ou, L. H. Vilela-Leao, D. C. Ralph, and R. A. Buhrman, *Phys Rev B* **92**, 064426 (2015).
- [11] P. M. Haney, H. W. Lee, K. J. Lee, A. Manchon, and M. D. Stiles, *Phys Rev B* **87**, 174411

(2013).

- [12] J. C. Rojas-Sanchez *et al.*, Phys Rev Lett **112**, 106602 (2014).
- [13] M. H. Nguyen, D. C. Ralph, and R. A. Buhrman, Phys Rev Lett **116**, 126601 (2016).
- [14] L. Q. Liu, T. Moriyama, D. C. Ralph, and R. A. Buhrman, Phys Rev Lett **106**, 036601 (2011).
- [15] C.-F. Pai, L. Q. Liu, Y. Li, H. W. Tseng, D. C. Ralph, and R. A. Buhrman, Appl Phys Lett **101**, 122404 (2012).
- [16] M.-H. Nguyen, M. Zhao, D. C. Ralph, and R. A. Buhrman, Appl Phys Lett **108**, 242407 (2016).
- [17] M. Obstbaum *et al.*, Phys Rev Lett **117**, 167204 (2016).
- [18] Y. X. Ou, S. J. Shi, D. C. Ralph, and R. A. Buhrman, Phys Rev B **93**, 220405 (2016).
- [19] P. Laczkowski *et al.*, Appl Phys Lett **104**, 142403 (2014).
- [20] K. U. Demasius, T. Phung, W. F. Zhang, B. P. Hughes, S. H. Yang, A. Kellock, W. Han, A. Pushp, and S. S. P. Parkin, Nat Commun **7**, 10644 (2016).
- [21] H. An, Y. Kageyama, Y. Kanno, N. Enishi, and K. Ando, Nat Commun **7**, 13069 (2016).
- [22] Y. Niimi, Y. Kawanishi, D. H. Wei, C. Deranlot, H. X. Yang, M. Chshiev, T. Valet, A. Fert, and Y. Otani, Phys Rev Lett **109**, 156602 (2012).
- [23] C. F. Pai, M. Mann, A. J. Tan, and G. S. D. Beach, Phys Rev B **93** (2016).
- [24] Y. X. Ou, D. C. Ralph, and R. A. Buhrman, Appl Phys Lett **110**, 192403 (2017).
- [25] C. T. Lin and K. L. Lin, Mater Chem Phys **82**, 306 (2003).
- [26] B. Dieny and M. Chshiev, Rev Mod Phys **89**, 025008 (2017).
- [27] Q. Hao and G. Xiao, Physical Review Applied **3**, 034009 (2015).
- [28] L. Q. Liu, O. J. Lee, T. J. Gudmundsen, D. C. Ralph, and R. A. Buhrman, Phys Rev Lett **109**, 096602 (2012).
- [29] O. J. Lee, L. Q. Liu, C. F. Pai, Y. Li, H. W. Tseng, P. G. Gowtham, J. P. Park, D. C. Ralph, and R. A. Buhrman, Phys Rev B **89**, 024418 (2014).
- [30] J. Finley and L. Liu, Physical Review Applied **6**, 054001 (2016).
- [31] K. Ueda, M. Mann, C.-F. Pai, A.-J. Tan, and G. S. D. Beach, Appl Phys Lett **109**, 232403 (2016).
- [32] A. Thiaville, S. Rohart, E. Jue, V. Cros, and A. Fert, Europhys. Lett. **100**, 57002 (2012).
- [33] R. Karplus and J. M. Luttinger, Phys Rev **95**, 1154 (1954).
- [34] T. Tanaka, H. Kontani, M. Naito, T. Naito, D. S. Hirashima, K. Yamada, and J. Inoue, Phys Rev B **77**, 165117 (2008).
- [35] Q. Hao and G. Xiao, Phys Rev B **91**, 224413 (2015).
- [36] E. Sagasta, Y. Omori, M. Isasa, M. Gradhand, L. E. Hueso, Y. Niimi, Y. Otani, and F. Casanova, Phys Rev B **94**, 060412 (2016).

- [37] K. S. Lee, S. W. Lee, B. C. Min, and K. J. Lee, *Appl Phys Lett* **102**, 112410 (2013).
- [38] D. Bhowmik, M. E. Nowakowski, L. You, O. Lee, D. Keating, M. Wong, J. Bokor, and S. Salahuddin, *Sci Rep-Uk* **5**, 11823 (2015).
- [39] J. Sinha *et al.*, *Appl Phys Lett* **102**, 242405 (2013).
- [40] J. Torrejon, F. Garcia-Sanchez, T. Taniguchi, J. Sinha, S. Mitani, J. V. Kim, and M. Hayashi, *Phys Rev B* **91**, 214434 (2015).

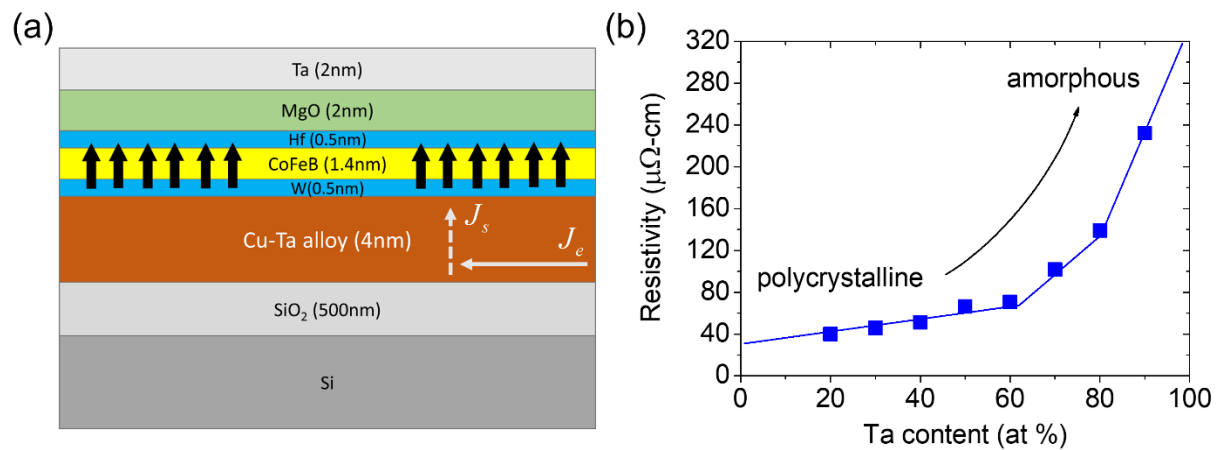


Figure 1. (a) Schematic illustration of the Cu-Ta alloy-based magnetic heterostructure. The black arrows represent the magnetic moment with desirable perpendicular magnetic anisotropy (PMA). J_e and J_s represent the vectors of longitudinal charge current and the transverse spin current, respectively (b) Resistivity of the co-sputtered $\text{Cu}_{100-x}\text{Ta}_x$ layer as a function of Ta content (atomic percentage).

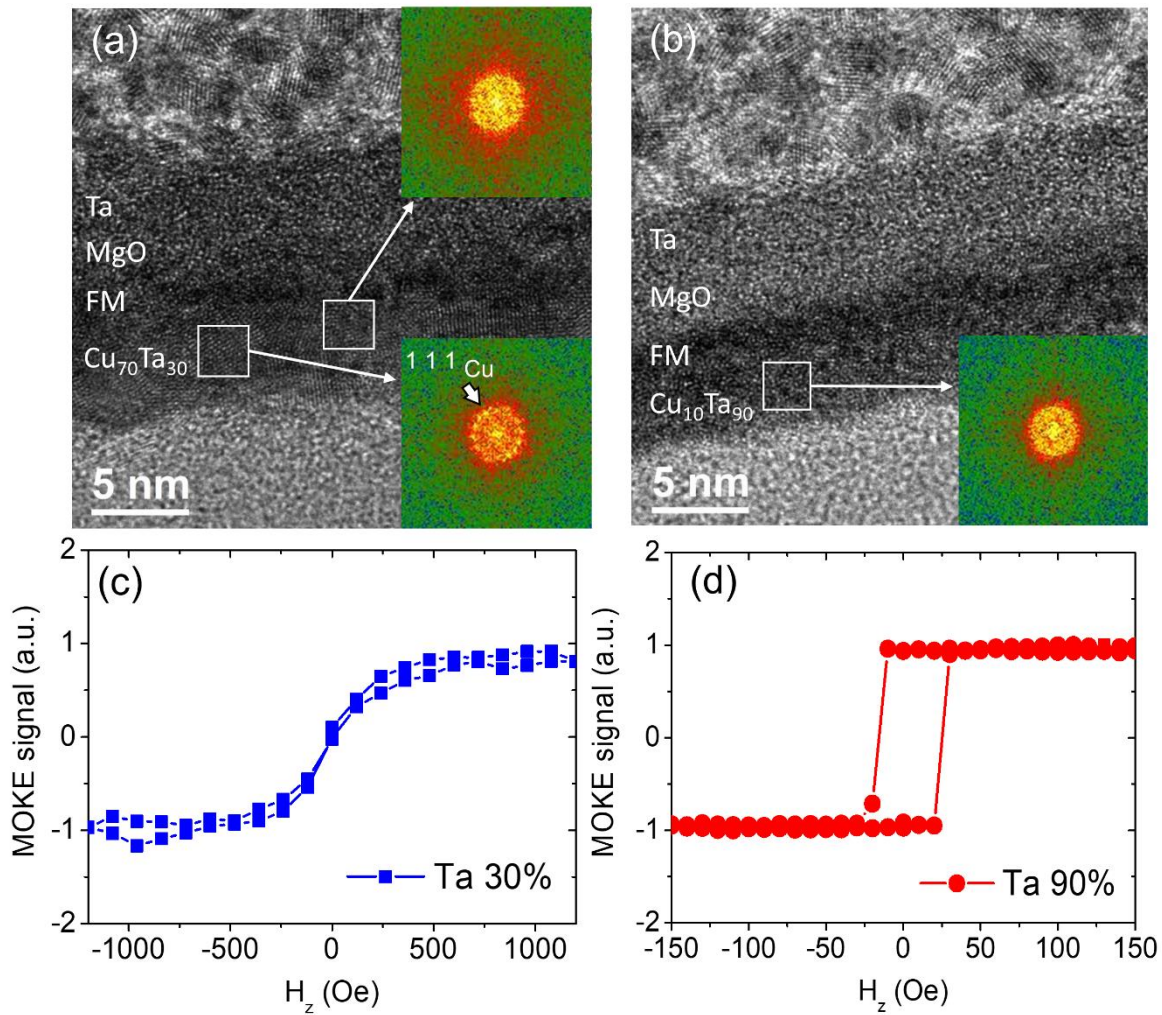


Figure 2. Cross section HR-TEM imaging results from (a) Cu₇₀Ta₃₀-based (Cu-rich) and (b) Cu₁₀Ta₉₀-based (Ta-rich) magnetic heterostructures. The subpanels show the diffractograms computed by reduced fast Fourier transformation (FFT) from the regions of interests. FM represents the effective ferromagnetic layer. Out-of-plane hysteresis loops of (c) Cu₇₀Ta₃₀-based (Cu-rich) and (d) Cu₁₀Ta₉₀-based (Ta-rich) magnetic heterostructures.

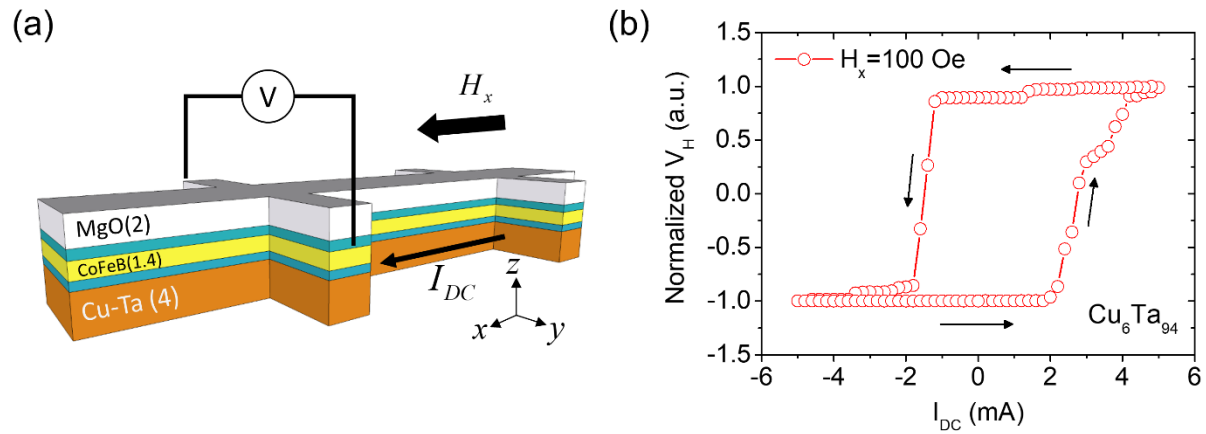


Figure 3. (a) Schematic illustration of a $\text{Cu}_{100-x}\text{Ta}_x$ -based ($84 \leq x \leq 100$) Hall-bar device and the application of in-plane field H_x as well as charge current I_{DC} for current-induced SOT switching measurements. (b) A representative current-induced SOT switching curve of a $\text{Cu}_6\text{Ta}_{94}(4)/\text{W}(0.5)/\text{CoFeB}(1.4)/\text{Hf}(0.5)/\text{MgO}(2)$ Hall-bar device under in-plane bias field $H_x = 100$ Oe. The black arrows indicate applied current scan directions.

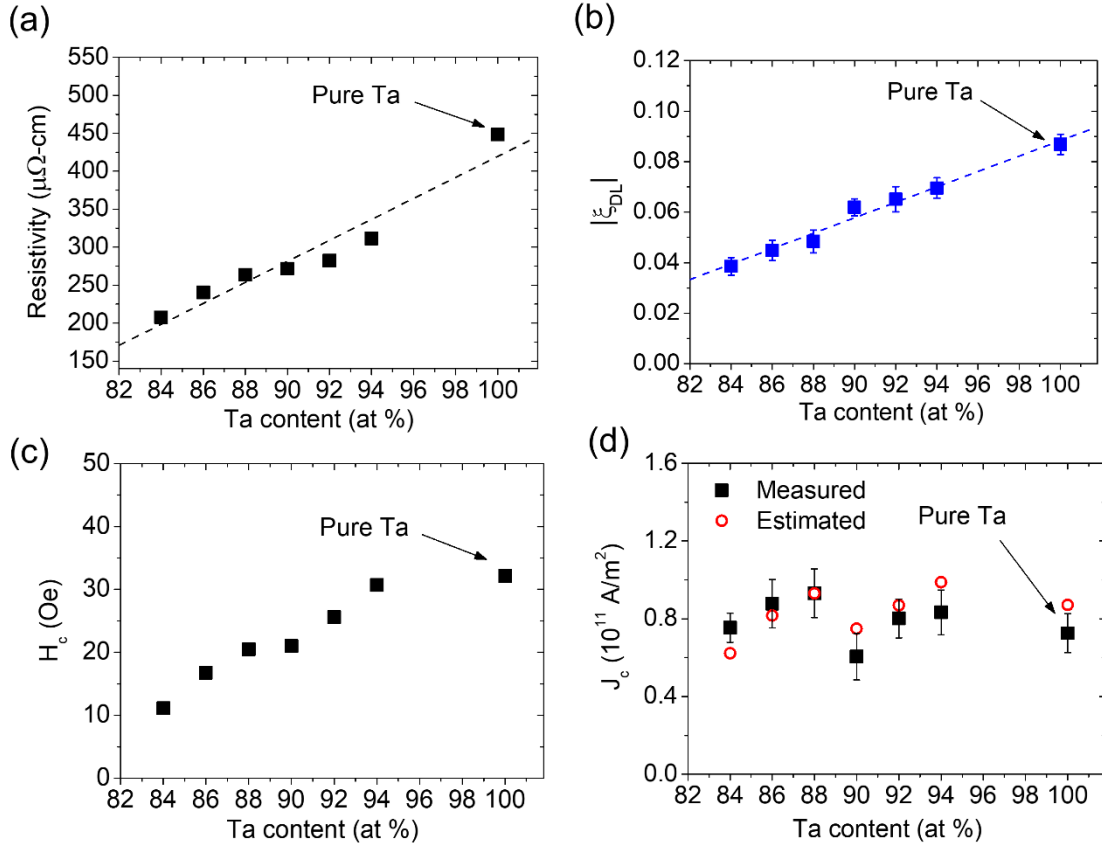


Figure 4. (a) Cu_{100-x}Ta_x buffer layer resistivity, (b) the DL-SOT efficiency $|\xi_{DL}|$ of Cu_{100-x}Ta_x-based magnetic heterostructures, (c) coercive field H_c of the magnetic layer, and (d) critical current density J_c for current-induced SOT switching as functions of Ta content in the Ta-rich regime ($x \geq 84$). The dashed lines in (a) and (b) are linear fits to experimental data. The estimated results of J_c (open red circles) in panel (d) are obtained from the experimental data in panels (b) and (c) through Eqn. (1).

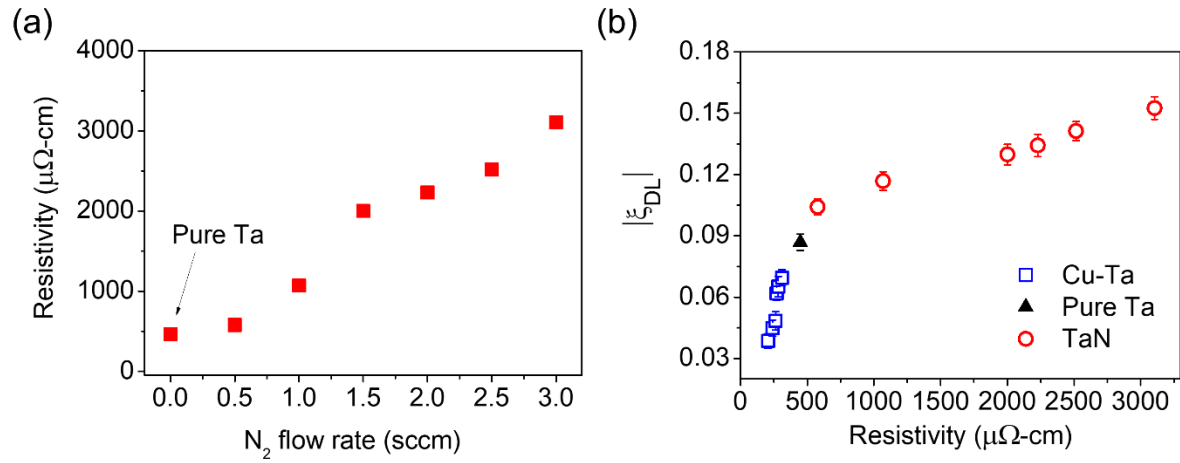


Figure 5. (a) TaN buffer layer resistivity as a function of N_2 flow rate during deposition. (b) A summary of characterized DL-SOT efficiency $|\xi_{DL}|$ as a function of buffer layer resistivity, for both alloying (Cu-Ta) and nitridation (TaN) samples.